

Shubnikov-de Haas and de Haas-van Alphen oscillations in topological semimetal CaAl_4

Sheng Xu,* Jian-Feng Zhang,* Yi-Yan Wang[†],* Lin-Lin Sun[‡], Huan

Wang, Yuan Su, Xiao-Yan Wang, Kai Liu, and Tian-Long Xia[§]

Department of Physics, Renmin University of China, Beijing 100872, P. R. China and
Beijing Key Laboratory of Opto-electronic Functional Materials & Micro-nano Devices,

Renmin University of China, Beijing 100872, P. R. China

(Dated: November 16, 2018)

We report the magneto-transport properties of CaAl_4 single crystals with $C2/m$ structure at low temperature. CaAl_4 exhibits large unsaturated magnetoresistance $\sim 3000\%$ at 2.5 K and 14 T. The nonlinear Hall resistivity is observed, which indicates the multi-band feature. The first-principles calculations show the electron-hole compensation and the complex Fermi surface in CaAl_4 , to which the two-band model with over-simplified carrier mobility can't completely apply. Evident quantum oscillations have been observed with $B//c$ and $B//ab$ configurations, from which the nontrivial Berry phase is extracted by the multi-band Lifshitz-Kosevich formula fitting. An electron-type quasi-2D Fermi surface is found by the angle-dependent Shubnikov-de Haas oscillations, de Haas-van Alphen oscillations and the first-principles calculations. The calculations also elucidate that CaAl_4 owns a Dirac nodal line type band structure around the Γ point in the $Z-\Gamma-L$ plane, which is protected by the mirror symmetry as well as the space inversion and time reversal symmetries. Once the spin-orbit coupling is included, the crossed nodal line opens a negligible gap (less than 3 meV). The open-orbit topology is also found in the electron-type Fermi surfaces, which is believed to help enhance the magnetoresistance observed.

I. INTRODUCTION

Topological semimetals have been a recent research focus due to their novel properties in condensed matter physics. Dirac semimetals display a four-fold degenerate Dirac point with two linear crossing bands¹. Cd_3As_2 ²⁻⁷ and Na_3Bi ⁸⁻¹¹ are the typical Dirac semimetals. Once the space inversion or time reversal symmetry is broken, the Dirac semimetals will evolve into Weyl semimetals^{12,13} like TaAs family¹⁴⁻²⁵ or $\text{SrMnSb}_2/\text{YbMnPn}_2$ ($\text{Pn}=\text{Sb}$ and Bi)²⁶⁻²⁹. Different from the Dirac and Weyl semimetals, PbTaSe_2 ³⁰ and ZrSiS family³¹⁻³³ possess a one-dimensional loop band touching, which are known as the nodal-line semimetals³⁴. All of these topological semimetals have demonstrated interesting transport properties. Lately, transition-metal dipnictides XPn_2 ($\text{X}=\text{Nb}$ or Ta ; $\text{Pn}=\text{As}$ or Sb) with $C2/m$ structure have attracted tremendous attention due to the novel phenomena such as resistivity plateau, extremely large magnetoresistance (MR) and negative longitudinal MR *etc.*³⁵⁻⁴⁰. It is believed that the extremely large MR in XPn_2 may originate from the electron-hole compensation, while the other mechanism may enhance it³⁵⁻⁴².

Motivated by previous results and discussions, we grew the high-quality CaAl_4 single crystals with the space group $C2/m$ at room temperature and studied its transport properties and electronic structure in details. The first-principles calculations reveal that there is a Dirac nodal line around the Γ point in the $Z-\Gamma-L$ plane, which is protected by the mirror symmetry as well as the space inversion and time reversal symmetries. However, the crossed nodal line opens a negligible gap (less than 3 meV) once the spin-orbit coupling (SOC) is included. Interestingly, an electron-type quasi-2D Fermi

surface (FS) is observed, which plays an important role in the magneto-transport properties. Magneto-transport measurements on CaAl_4 display a large unsaturated MR up to 3000% at 2.5 K and 14 T. The nonlinear and negative Hall resistivity indicate the multi-band and electron dominant features, which is slightly in disagreement with the calculations. According to the analysis of the two-band model, the electron-hole un-compensation is expected, while the calculations suggest that the electron and hole are compensated. The mismatch is discussed in the main text of this paper. Besides, evident Haas-van Alphen oscillations (dHvA) and Shubnikov-de Haas oscillations (SdH) have been observed at low temperature and high magnetic field. Three fundamental frequencies have been extracted after the fast Fourier transform (FFT) analysis with $B//c$ configuration. The multi-band Lifshitz-Kosevich (LK) formula fitting yields the nontrivial Berry phase. Angle-dependent SdH oscillations reveal that the γ pocket displays quasi-2D characteristic which is in agreement with the calculations.

II. METHODS AND CRYSTAL STRUCTURE

The high quality single crystals of CaAl_4 were grown by the self-flux method. The calcium and aluminum granules were put into the crucible and sealed into a quartz tube with the ratio $\text{Ca}:\text{Al}=14:86$. The quartz tube was heated to 900°C , then cooled to 690°C in 70 hours, and to 660°C in 30 hours. The excess flux was removed by centrifugation. The atomic composition of CaAl_4 single crystal was checked to be $\text{Ca}:\text{Al}=1:4$ by energy dispersive x-ray spectroscopy (EDS, Oxford X-Max 50). The single-crystal x-ray diffraction (XRD) pattern and temperature dependent powder XRD patterns were collected from a Bruker D8 Advance x-ray diffractometer using $\text{Cu } K_\alpha$ radiation. TOPAS-4.2 was employed for the refinement. The measurements of resistivity and magnetic properties were performed on a Quantum Design physical property

[†]Present address: Institute of Physics, Chinese Academy of Sciences.

[‡]Present address: Pinggu Branch of High School Affiliated to Beijing Normal University.

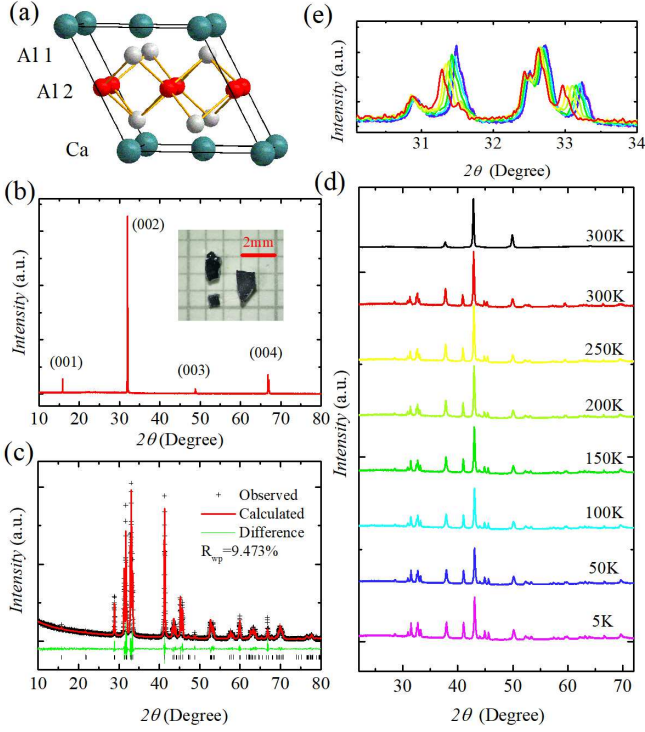


FIG. 1: (a) Crystal structure of CaAl_4 at room temperature. (b) Single crystal XRD pattern of CaAl_4 at room temperature. Inset shows the picture of selected crystals. (c) Powder XRD pattern and the Rietveld refinement of CaAl_4 . The value of R_{wp} is 9.413%. (d), (e) Powder XRD patterns and the enlargement part of CaAl_4 with the background of the platform (The curve in black at 300 K) at different temperatures.

measurement system (QD PPMS-14T). The electronic structure was studied by the first-principles calculations with the projector augmented wave (PAW) method^{43,44} as implemented in the VASP package⁴⁵⁻⁴⁷. For the exchange-correlation functional, the generalized gradient approximation (GGA) of the Perdew-Burke-Ernzerhof (PBE) formula⁴⁸ was adopted. The kinetic energy cutoff of the plane-wave basis was set to be 350 eV. A $20 \times 20 \times 20$ k -point mesh was utilized for the BZ sampling and the Fermi surface was broadened by the Gaussian smearing method with a width of 0.05 eV. The lattice parameters and internal atomic positions were fully relaxed until the forces on all atoms were smaller than 0.01 eV/Å. After the equilibrium structures were obtained, the electronic structures were calculated by including the SOC effect. The Fermi surfaces were studied by using the maximally localized Wannier functions (MLWF) method^{49,50}.

The crystal structure of CaAl_4 is reported to be $I4/mmm$ in the ICSD database. However, Miller *et al.* pointed out its structure transition from tetragonal to monoclinic at 443 K⁵¹ and its room temperature structure is $C2/m$ ⁵¹ which is the same as that of XPn_2 family. Figure 1(b) shows the XRD pattern of a single crystal at room temperature, which reveals the surface of the crystal is the $(00l)$ plane. The powder XRD pattern (the sample is crushed from the single crystals) is also checked and shown in Fig. 1(c) which can be well re-

fined with $C2/m$ (No.12) space group. The refined lattice parameters are $a = 6.1695\text{\AA}$, $b = 6.1842\text{\AA}$, $c = 6.3451\text{\AA}$ and $\beta = 118.0647^\circ$, which are in agreement with previous results⁵¹. In addition, the Young modulus indicated that there may exist another structure transition at $\sim 243\text{ K}$ ⁵². Thus, we performed the temperature dependent XRD measurements on CaAl_4 powder sample between 300 K and 5 K as shown in Figs. 1(d) and 1(e). The black line in Fig. 1(d) shows the XRD pattern of the sample platform at 300 K. The temperature dependent powder diffraction pattern does not change obviously [Fig. 1(e)], in which only the peak position of the specific crystal plane changes slightly to the higher 2θ value with the decreasing temperature [Fig. 1(e)], which originates from the decrease of the lattice parameters. Thus, there is no structure transition among this temperature range.

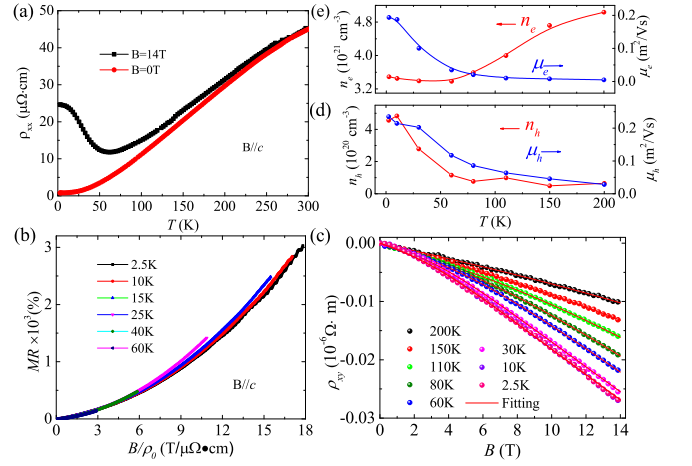


FIG. 2: (a) Temperature dependent resistivity of CaAl_4 at 0 T and 14 T. (b) The plot of MR as a function of B/ρ_0 at different temperatures. (c) Magnetic field dependent Hall resistivity at various temperatures. The red lines are the fitting results from the two-band model. (d), (e) Temperature dependence of carrier concentrations and mobility.

III. RESULTS AND DISCUSSIONS

Figure 2(a) exhibits the temperature dependent resistivity $\rho_{xx}(0)$ and $\rho_{xx}(14T)$. The $\rho_{xx}(0)$ shows metallic behaviour and the residual resistance ratio (RRR) equal to 57. The resistivity $\rho_{xx}(14T)$ shows an upturn below 60 K accompanied with a plateau. Figure 2(b) plots the magnetic field dependent MR at various temperatures when B is applied parallel to c -axis. The MR reaches 3000% at 2.5 K and 14 T which is comparable to that of type-II Weyl semimetal Ta_3S_2 ⁵³. The MR in Fig. 2(b) shows $B^{1.6}$ field dependence which violates the Kohler's rule, indicating the coexistence of electrons and holes⁵⁴. In order to thoroughly identify the characteristics of the carriers in CaAl_4 , we performed temperature dependent Hall resistivity measurements. The Hall resistivity ρ_{xy} curves of CaAl_4 at various temperatures from 2.5 K to 200 K are shown in Fig. 2(c). The two-band model is used to describe the Hall resistivity,

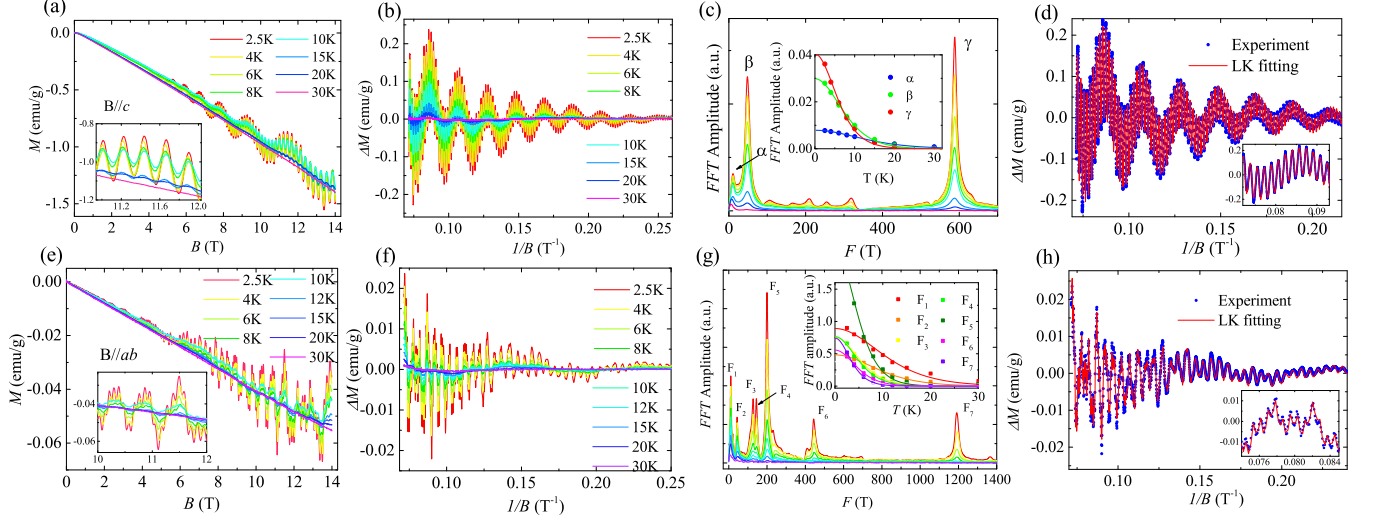


FIG. 3: (a), (e) The dHvA oscillations at various temperatures for $B//c$ and $B//ab$. (b), (f) The amplitudes of dHvA oscillations as a function of $1/B$. (c), (g) The FFT spectra of the oscillations. The insets are the temperature dependence of relative FFT amplitude of the main oscillation frequency. (d), (h) The fitting of dHvA oscillations at 2.5 K by the multi-band LK formula.

$$\rho_{xy} = \frac{B}{e} \frac{(n_h \mu_h^2 - n_e \mu_e^2) + (n_h - n_e)(\mu_h \mu_e)^2 B^2}{(n_h \mu_h + n_e \mu_e)^2 + (n_h - n_e)^2 (\mu_h \mu_e)^2 B^2} \quad (1)$$

where $n_{e,h}$ and $\mu_{e,h}$ represent the concentration and mobility of electrons and holes, respectively. The red lines in Fig. 2(c) are the fitting results, and the temperature dependent concentrations and mobility are plotted in Figs. 2(d) and 2(e). At 2.5 K, $n_e = 3.5 \times 10^{21} \text{cm}^{-3}$ and it is almost eight times larger than $n_h = 4.5 \times 10^{20} \text{cm}^{-3}$, and the μ_e and μ_h are $0.19 \text{m}^2/\text{V}^{-1}\text{s}^{-1}$ and $0.23 \text{m}^2/\text{V}^{-1}\text{s}^{-1}$, respectively. Nevertheless, the first-principles calculations indicate that the electron and hole are compensated with the concentrations $n_e \approx n_h = 1 \times 10^{21} \text{cm}^{-3}$. Both the quantum oscillations and the calculations confirmed the multi-band character in CaAl_4 , each of which shows different mobility. However, the two-band model simplified the mobility into a simple one $\mu_e \mu_h$, which leads to the disagreement of concentrations between the fitting and the calculations.

Quantum oscillation experiment is an effective method in the study of topological materials. CaAl_4 shows obvious dHvA oscillations, as shown in Figs. 3(a) and 3(e) with magnetic field up to 14 T. The dHvA oscillations are more distinct at lower temperature and higher field. After subtracting a smoothing background, the periodic oscillations $\Delta M = M - \langle M \rangle$ versus $1/B$ are shown in Fig. 3(b) for $B//c$ and 3(f) for $B//ab$, respectively. Three fundamental frequencies $F_\alpha = 10.7$ T, $F_\beta = 48.4$ T and $F_\gamma = 588.3$ T are obtained after the FFT analysis when the field is applied along c-axis. The number of FFT frequencies almost doubles when the field is applied along the ab-plane as presented in Table I, indicating the more complex FS cross sections along this direction. The oscillatory components versus $1/B$ of dHvA oscillations can be described by the LK formula⁵⁵:

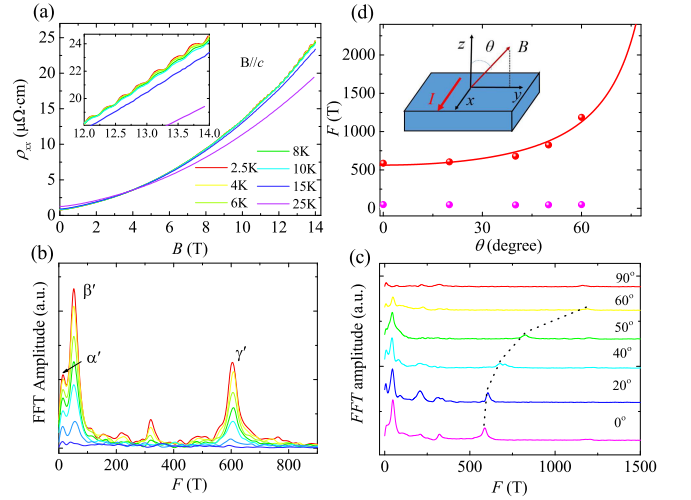


FIG. 4: (a) Resistivity $\rho_{xx}(B)$ as a function of field ($B//c$) at various temperatures. Inset shows the enlargement of the oscillations at high field. (b) The FFT spectra of SdH oscillations at different temperatures. (c) The FFT spectra of SdH oscillations with the field in different directions at 2.5 K. (d) Angle dependence of the frequencies. The solid line in red is the fitting curve with $F = F_0/\cos(\theta)$ for γ' pocket. The inset shows the definition of θ .

$$\Delta M \propto -B^{1/2} \frac{\lambda T}{\sinh(\lambda T)} e^{-\lambda T_D} \sin\left[2\pi\left(\frac{F}{B} - \frac{1}{2} + \beta + \delta\right)\right] \quad (2)$$

where $\lambda = (2\pi^2 k_B m^*)/(\hbar e B)$. T_D is the Dingle temperature. The value of δ depends on the dimensionality, $\delta = 0$ for the 2D system and $\delta = \pm 1/8$ for the 3D system. $\beta = \phi_B/2\pi$ and ϕ_B is the Berry phase. The insets of Figs. 3(c) and 3(g) show the temperature dependent FFT amplitudes and the fitting by the thermal factor $R_T = (\lambda T)/\sinh(\lambda T)$ in LK

TABLE I: The parameters extracted from dHvA oscillations in CaAl₄. F is the frequency of dHvA oscillations; m^*/m_e is the ratio of the effective mass to the electron mass; ϕ_B is the Berry phase.

		F(T)	m^*/m_e	$\phi_B(\delta=0)$	$\phi_B(\delta=-1/8)$	$\phi_B(\delta=1/8)$
B//c	α	10.7	0.07	/	1.15π	/
	β	48.4	0.12	/	0.34π	/
	γ	588.3	0.15	1.65π	/	/
B//ab	F ₁	10.9	0.06	/	1.57π	/
	F ₂	43.7	0.07	/	0.57π	/
	F ₃	127.5	0.13	0.06π	0.31π	-0.19π
	F ₄	144.5	0.14	1.61π	1.86π	1.36π
	F ₅	200.2	0.14	1.62π	1.87π	1.37π
	F ₆	444.5	0.15	1.39π	1.63π	1.13π
	F ₇	1192.5	0.20	0.87π	1.12π	0.62π

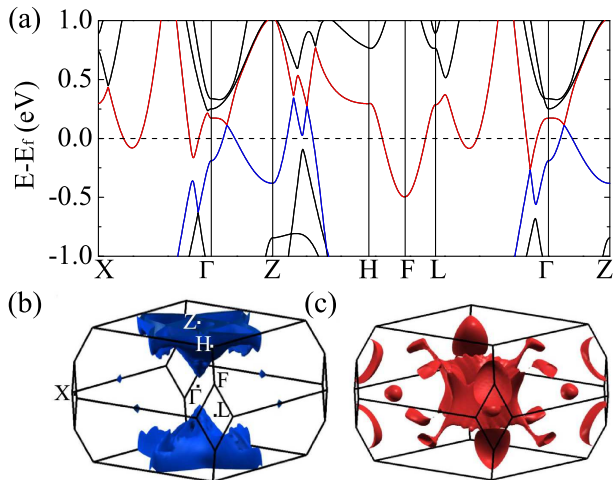


FIG. 5: (color online) (a) The band structure of CaAl₄ with SOC considered. (b),(c) The hole-like and electron-like Fermi surfaces of CaAl₄.

formula, from which the effective masses are obtained to be $m_\alpha^* = 0.07m_e$, $m_\beta^* = 0.12m_e$ and $m_\gamma^* = 0.15m_e$ (B//c). As is well known, topological non-trivial materials require a non-trivial π Berry phase, while for the trivial materials, the Berry phase equals 0 or 2π . In this work, it is a challenge to employ Landau level (LL) index fan diagram analysis since the oscillations contain too many frequencies. Thus, we applied multi-band LK formula fitting as displayed in Figs. 3(d) and 3(h). The obtained Berry phases of each pocket are exhibited in Table I, several of which are close to π indicating the possible topological non-trivial characteristic.

Figure 4(a) displays $\rho_{xx}(B)$ versus magnetic field at various temperatures. The CaAl₄ exhibits obvious SdH oscillations at low temperature and high field (B//c). The oscillations tend to disappear with the increasing temperature and almost vanish at 25 K. Fig. 4(b) shows the FFT frequencies $F'_\alpha=6.3$ T, $F'_\beta=53$ T and $F'_\gamma=605$ T of the SdH oscillations. The effective masses of these pockets are extracted to be $m_{F'_\alpha}^* = 0.07m_e$, $m_{F'_\beta}^* = 0.12m_e$ and $m_{F'_\gamma}^* = 0.13m_e$. Both the FFT frequencies and the relevant effective masses are comparable to that of dHvA oscillations with B//c configuration. In order to study

its electronic structure in details, we applied angle-dependent SdH oscillation measurements. The rotation angle is defined as $\theta=0^\circ$ for B//c, $\theta=90^\circ$ for B//ab and B is always perpendicular to the current I as shown in the insert of the Fig. 4(d). Figure 4(c) displays the FFT frequencies extracted from the SdH oscillations at different orientations. F'_γ shows an obvious angle dependent characteristic and is fitted by $F=A/\cos(\theta)$ as shown in Fig. 4(c), which implies the quasi-2D FS morphology.

The electronic structure of CaAl₄ with SOC is calculated and presented in Fig. 5(a). The first-principles calculations elucidate that CaAl₄ owns a Dirac nodal line around the Γ point in the Z - Γ - L plane, which is protected by the mirror symmetry as well as the space inversion and time reversal symmetries. When the SOC is considered, the crossed nodal line opens a negligible gap which is less than 3 meV. This negligible gap almost has no effect on the topological properties, especially in the magneto-transport measurements. Figures 5(b) and 5(c) display the hole-type and electron-type FSs, respectively, where the electron-type FSs contain a quasi-2D FS [Fig. 5(c)] which coincides with the result of the transport measurements.

IV. SUMMARY

In conclusion, we synthesized the single crystals of CaAl₄ and confirmed its crystal structure as $C2/m$ at low temperature. The possible secondary structure transition at ~ 243 K indicated in previous results is not observed. The large MR reaches $\sim 3000\%$ at 2.5 K and 14 T. The multi-band feature is revealed by the analysis of Hall resistivity and the first-principles calculations. The disagreement between the two-band model fitting and the calculations comes from the over-simplified model. Evident dHvA oscillations have been observed, from which the nontrivial Berry phase is extracted from the multi-band LK formula fitting. CaAl₄ possesses a Dirac nodal ring type band structure around Γ point, which is protected by the mirror symmetry as well as the space inversion and time reversal symmetries. The crossed nodal line opens a negligible gap (less than 3 meV) when the SOC is included, which almost has no influence on the topological properties in the magneto-transport measurements. A quasi-2D electron-type FS is found by the angle-dependent SdH oscillations, in agreement with the calculations. The carrier compensation and topological nontrivial bands with high carrier mobility are believed to result in the large MR in CaAl₄, while the observed open-orbit topology in part of the quasi-2D Fermi surface helps enhance it.

V. ACKNOWLEDGMENTS

We thank Peng-Jie Guo for helpful discussions. This work is supported by the National Natural Science Foundation of China (No.11574391, No.11874422, No.11774424), the Fundamental Research Funds for the Central Universities, and the Research Funds of Renmin University of China

(No.18XNLG14). Computational resources have been provided by the Physical Laboratory of High Performance Com-

puting at Renmin University of China. The Fermi surfaces were prepared with the XCRYSDEN program⁵⁶.

* These authors contributed equally to this paper

[§] Electronic address: tlxia@ruc.edu.cn

- ¹ T. Wehling, A. M. Black-Schaffer, and A. V. Balatsky, *Adv. Phys.* **63**, 1 (2014).
- ² M. Neupane, S.-Y. Xu, R. Sankar, N. Alidoust, G. Bian, C. Liu, I. Belopolski, T.-R. Chang, H.-T. Jeng, H. Lin, *et al.*, *Nat. Commun.* **5**, 3786 (2014).
- ³ Z. Liu, J. Jiang, B. Zhou, Z. Wang, Y. Zhang, H. Weng, D. Prabhakaran, S. Mo, H. Peng, P. Dudin, *et al.*, *Nat. Mater.* **13**, 677 (2014).
- ⁴ S. Borisenko, Q. Gibson, D. Evtushinsky, V. Zabolotnyy, B. Büchner, and R. J. Cava, *Phys. Rev. Lett.* **113**, 027603 (2014).
- ⁵ T. Liang, Q. Gibson, M. N. Ali, M. Liu, R. Cava, and N. Ong, *Nat. Mater.* **14**, 280 (2015).
- ⁶ C.-Z. Li, L.-X. Wang, H. Liu, J. Wang, Z.-M. Liao, and D.-P. Yu, *Nat. Commun.* **6**, 10137 (2015).
- ⁷ H. Li, H. He, H. Lu, H. Zhang, H. Liu, R. Ma, Z. Fan, S. Shen, and J. Wang, *Nat. Commun.* **7**, 10301 (2015).
- ⁸ Z. Wang, Y. Sun, X.-Q. Chen, C. Franchini, G. Xu, H. Weng, X. Dai, and Z. Fang, *Phys. Rev. B* **85**, 195320 (2012).
- ⁹ Z. Liu, B. Zhou, Y. Zhang, Z. Wang, H. Weng, D. Prabhakaran, S.-K. Mo, Z. Shen, Z. Fang, X. Dai, *et al.*, *Science* **343**, 864 (2014).
- ¹⁰ J. Xiong, S. K. Kushwaha, T. Liang, J. W. Krizan, M. Hirschberger, W. Wang, R. Cava, and N. Ong, *Science* **350**, 413 (2015).
- ¹¹ J. Xiong, S. Kushwaha, J. Krizan, T. Liang, R. Cava, and N. Ong, *EPL* **114**, 27002 (2016).
- ¹² X. Wan, A. M. Turner, A. Vishwanath, and S. Y. Savrasov, *Phys. Rev. B* **83**, 205101 (2011).
- ¹³ Z. Fang, N. Nagaosa, K. S. Takahashi, A. Asamitsu, R. Mathieu, T. Ogasawara, H. Yamada, M. Kawasaki, Y. Tokura, and K. Terakura, *Science* **302**, 92 (2003).
- ¹⁴ H. Weng, C. Fang, Z. Fang, B. A. Bernevig, and X. Dai, *Phys. Rev. X* **5**, 011029 (2015).
- ¹⁵ S.-Y. Xu, I. Belopolski, N. Alidoust, M. Neupane, G. Bian, C. Zhang, R. Sankar, G. Chang, Z. Yuan, C.-C. Lee, *et al.*, *Science* **349**, 613 (2015).
- ¹⁶ S.-M. Huang, S.-Y. Xu, I. Belopolski, C.-C. Lee, G. Chang, B. Wang, N. Alidoust, G. Bian, M. Neupane, C. Zhang, *et al.*, *Nat. Commun.* **6**, 7373 (2015).
- ¹⁷ B. Lv, H. Weng, B. Fu, X. Wang, H. Miao, J. Ma, P. Richard, X. Huang, L. Zhao, G. Chen, *et al.*, *Phy. Rev. X* **5**, 031013 (2015).
- ¹⁸ B. Q. Lv, N. Xu, H. M. Weng, J. Z. Ma, P. Richard, X. C. Huang, L. X. Zhao, G. F. Chen, C. E. Matt, F. Bisti, V. N. Strocov, J. Mesot, Z. Fang, X. Dai, T. Qian, M. Shi, and H. Ding, *Nat. Phys.* **11**, 724 (2015).
- ¹⁹ S.-Y. Xu, N. Alidoust, I. Belopolski, Z. Yuan, G. Bian, T.-R. Chang, H. Zheng, V. N. Strocov, D. S. Sanchez, G. Chang, *et al.*, *Nat. Phys.* **11**, 748 (2015).
- ²⁰ S.-Y. Xu, I. Belopolski, D. S. Sanchez, C. Zhang, G. Chang, C. Guo, G. Bian, Z. Yuan, H. Lu, T.-R. Chang, *et al.*, *Sci. Adv.* **1**, e1501092 (2015).
- ²¹ N. Xu, H. Weng, B. Lv, C. Matt, J. Park, F. Bisti, V. Strocov, D. Gawryluk, E. Pomjakushina, K. Conder, *et al.*, *Nat. Commun.* **7** (2016).
- ²² Z. Liu, L. Yang, Y. Sun, T. Zhang, H. Peng, H. Yang, C. Chen, Y. Zhang, Y. f Guo, D. Prabhakaran, *et al.*, *Nat. Mater.* **15**, 27 (2016).
- ²³ X. Huang, L. Zhao, Y. Long, P. Wang, D. Chen, Z. Yang, H. Liang, M. Xue, H. Weng, Z. Fang, *et al.*, *Phys. Rev. X* **5**, 031023 (2015).
- ²⁴ C.-L. Zhang, S.-Y. Xu, I. Belopolski, Z. Yuan, Z. Lin, B. Tong, G. Bian, N. Alidoust, C.-C. Lee, S.-M. Huang, *et al.*, *Nat. Commun.* **7** (2016).
- ²⁵ F. Arnold, C. Shekhar, S.-C. Wu, Y. Sun, R. D. Dos Reis, N. Kumar, M. Naumann, M. O. Ajeesh, M. Schmidt, A. G. Grushin, *et al.*, *Nat. Commun.* **7** (2016).
- ²⁶ J. Liu, J. Hu, Q. Zhang, D. Graf, H. B. Cao, S. Radmanesh, D. Adams, Y. Zhu, G. Cheng, X. Liu, *et al.*, *Nat. Mater.* **16**, 905 (2017).
- ²⁷ S. Borisenko, D. Evtushinsky, Q. Gibson, A. Yaresko, T. Kim, M. Ali, B. Buechner, M. Hoesch, and R. J. Cava, arXiv preprint arXiv:1507.04847 (2015).
- ²⁸ Y.-Y. Wang, S. Xu, L.-L. Sun, and T.-L. Xia, *Phys. Rev. Mater.* **2**, 021201 (2018).
- ²⁹ R. Kealhofer, S. Jang, S. M. Griffin, C. John, K. A. Benavides, S. Doyle, T. Helm, P. J. Moll, J. B. Neaton, J. Y. Chan, *et al.*, *Phys. Rev. B* **97**, 045109 (2018).
- ³⁰ G. Bian, T.-R. Chang, R. Sankar, S.-Y. Xu, H. Zheng, T. Neupert, C.-K. Chiu, S.-M. Huang, G. Chang, I. Belopolski, *et al.*, *Nat. Commun.* **7**, 10556 (2016).
- ³¹ Q. Xu, Z. Song, S. Nie, H. Weng, Z. Fang, and X. Dai, *Phys. Rev. B* **92**, 205310 (2015).
- ³² J. Hu, Z. Tang, J. Liu, X. Liu, Y. Zhu, D. Graf, K. Myhro, S. Tran, C. N. Lau, J. Wei, *et al.*, *Phys. Rev. Lett.* **117**, 016602 (2016).
- ³³ N. Kumar, K. Manna, Y. Qi, S.-C. Wu, L. Wang, B. Yan, C. Felser, and C. Shekhar, *Phys. Rev. B* **95**, 121109 (2017).
- ³⁴ A. Burkov, M. Hook, and L. Balents, *Phys. Rev. B* **84**, 235126 (2011).
- ³⁵ Y.-Y. Wang, Q.-H. Yu, P.-J. Guo, K. Liu, and T.-L. Xia, *Phys. Rev. B* **94**, 041103 (2016).
- ³⁶ D. Wu, J. Liao, W. Yi, X. Wang, P. Li, H. Weng, Y. Shi, Y. Li, J. Luo, X. Dai, *et al.*, *Appl. Phys. Lett.* **108**, 042105 (2016).
- ³⁷ Z. Yuan, H. Lu, Y. Liu, J. Wang, and S. Jia, *Phys. Rev. B* **93**, 184405 (2016).
- ³⁸ B. Shen, X. Deng, G. Kotliar, and N. Ni, *Phys. Rev. B* **93**, 195119 (2016).
- ³⁹ Y. Luo, R. McDonald, P. Rosa, B. Scott, N. Wakeham, N. Ghimire, E. Bauer, J. Thompson, and F. Ronning, *Sci Rep* **6**, 27294 (2016).
- ⁴⁰ Y. Li, L. Li, J. Wang, T. Wang, X. Xu, C. Xi, C. Cao, and J. Dai, *Phys. Rev. B* **94**, 121115 (2016).
- ⁴¹ P.-J. Guo, H.-C. Yang, B.-J. Zhang, K. Liu, and Z.-Y. Lu, *Phys. Rev. B* **93**, 235142 (2016).
- ⁴² R. Lou, Y. Xu, L.-X. Zhao, Z.-Q. Han, P.-J. Guo, M. Li, J.-C. Wang, B.-B. Fu, Z.-H. Liu, Y.-B. Huang, *et al.*, *Phys. Rev. B* **96**, 241106 (2017).
- ⁴³ P. E. Blöchl, *Phys. Rev. B* **50**, 17953 (1994).
- ⁴⁴ G. Kresse and D. Joubert, *Phys. Rev. B* **59**, 1758 (1999).
- ⁴⁵ G. Kresse and J. Hafner, *Phys. Rev. B* **47**, 558 (1993).
- ⁴⁶ G. Kresse and J. Furthmüller, *Comp. Mater. Sci.* **6**, 15 (1996).
- ⁴⁷ G. Kresse and J. Furthmüller, *Phys. Rev. B* **54**, 11169 (1996).
- ⁴⁸ J. P. Perdew, K. Burke, and M. Ernzerhof, *Phys. Rev. Lett.* **77**, 3865 (1996).
- ⁴⁹ N. Marzari and D. Vanderbilt, *Phys. Rev. B* **56**, 12847 (1997).

- ⁵⁰ I. Souza, N. Marzari, and D. Vanderbilt, *Phys. Rev. B* **65**, 035109 (2001).
- ⁵¹ G. J. Miller, F. Li, and H. F. Franzen, *J. Am. Chem. Soc.* **115**, 3739 (1993).
- ⁵² H. Zogg and P. Schwelling, *J. Mater. Sci.* **14**, 1923 (1979).
- ⁵³ D. Chen, L. Zhao, J. He, H. Liang, S. Zhang, C. Li, L. Shan, S. Wang, Z. Ren, C. Ren, *et al.*, *Phys. Rev. B* **94**, 174411 (2016).
- ⁵⁴ R. H. McKenzie, J. Qualls, S. Han, and J. Brooks, *Phys. Rev. B* **57**, 11854 (1998).
- ⁵⁵ D. Shoenberg, *Magnetic oscillations in metals* (Cambridge University Press, 2009).
- ⁵⁶ A. Kokalj, *Comp. Mater. Sci.* **28**, 155 (2003).